A High Order Kinetic Flux-Splitting Method for the Special Relativistic Hydrodynamics *

Shamsul Qamar † and Gerald Warnecke ‡

Institute for Analysis and Numerics, Otto-von-Guericke University

PSF 4120, D-39106 Magdeburg, Germany

May 11, 2004

Abstract. In this article we present a flux splitting method based on gas-kinetic theory for the special relativistic hydrodynamics (SRHD) [Landau & Lifshitz, Fluid Mechanics, Pergamon New York, 1987] in one and two space dimensions. This kinetic method is based on the direct splitting of the macroscopic flux functions with the consideration of particle transport. At the same time, particle "collisions" are implemented in the free transport process to reduce numerical dissipation. Due to the nonlinear relations between conservative and primitive variables and the consequent complexity of the Jacobian matrix, the multi-dimensional shock-capturing numerical schemes for SRHD are computationally more expensive. All the previous methods presented for the solution of these equations were based on the macroscopic continuum description. These upwind high-resolution shock-capturing (HRSC) schemes, which were originally made for non-relativistic flows, were extended to SRHD. However our method, which is based on kinetic theory is more related to the physics of these equations and is very efficient, robust, and easy to implement. In order to get high order accuracy in space, we use a third order central weighted essentially non-oscillatory (CWENO) finite difference interpolation routine. To achieve high order accuracy in time we use a Runge-Kutta time stepping method. The one- and two-dimensional computations reported in this paper show the desired accuracy, high resolution, and robustness of the method.

Mathematics Subject Classification (2000): 65M99, 76Y05, 85A30.

Keywords: Special relativistic hydrodynamics, kinetic flux-splitting method, high order reconstruction, conservation laws, hyperbolic systems, discontinuous solutions.

*This research was supported by the German Research Foundation under DFG Contract Nos. WA633/6-3 and WA633/10-3.

†Shamsul.Qamar@Mathematik.Uni-Magdeburg.DE

‡Gerald.Warnecke@Mathematik.Uni-Magdeburg.DE

1 Introduction

Relativistic flows and shocks play an essential role in modern high energy astrophysics, both for interpretation of various observed features and for the description of physical process to which they give rise. For example, relativistic jets which result from accretion onto compact objects, and gamma-ray bursts (GRB's) can be modeled with the use of special relativistic hydrodynamics (SRHD), see Aloy et al. [1] and Piran et al. [27]. GRB's are high-energy explosions of not yet determined objects in the universe, at cosmological distances from the earth. The other application fields of SRHD are the high energy particles beams and free-electron laser technology. Also in the field of heavy-ion collisions SRHD can be applied, see Csernai [3]. The ions are then modeled as droplets of fluid whose properties are governed by a nuclear equation of state. The necessity of modeling such relativistic flows which also involve strong shocks is triggering the development of relativistic hydro-codes.

In the relativistic case, space and time are coupled and the SRHD equations of gas dynamics become more complicated as compared to the classical ones. Due to the nonlinear relations between conservative and primitive variables and the consequent complexity of the Jacobian matrix, the multi-dimensional shock-capturing numerical schemes for SRHD are computationally more expensive.

During the last decade several upwind high-resolution shock-capturing (HRSC) schemes, which were originally derived for non-relativistic flows, were being applied to relativistic Euler equations too. These schemes achieve both high accuracy in smooth regions of the simulated flow and sharp discontinuous profiles in the shocks, see for example, Aloy et al. [1], Donat & Marquina [6], Eulderink & Mellema [7], Martí & Müller [21, 23], Schneider et al. [29], and Del Zana et al. [39]. Except for the kinetic beam scheme of Yang et al. [38], all these methods are based on the macroscopic continuum description.

On the other hand, Kunik, Qamar & Warnecke [14, 15, 16] have used kinetic schemes in order to solve the special relativistic Euler equations. These relativistic Euler equations result directly from the moments of the relativistic Jüttner equilibrium phase density [12] without taking any approximations. In these articles, we have derived the ultra-relativistic and general form of special relativistic Euler equations. However, in these articles we have mostly concentrated on the ultra-relativistic case. At that time we were unable to find a consistent kinetic phase density and its moments which can recover all the constitutive relations of the SRHD equations [17] presented in this article and in the articles of above paragraph.

In this article we present a gas-kinetic flux splitting method in order to solve the SRHD equations [17]. According to our knowledge we are the first to solve these Euler equation with a kinetic flux splitting method. We will modify the ultra-relativistic phase density and its moments [14] in order to recover all the constitutive relations of these special relativistic Euler equations. The use of a modified ultra-phase density has a significant advantage due to its simplicity as compared to the general relativistic phase density of Jüttner [12]. We will follow the same technique which was used by Xu [36] as will as Tang & Xu [30] for the classical phase density in the classical MHD equations solution. The scheme is based on the BGK-type formulation which generalize the KFVS scheme for SRHD equations by including particle collisions. As a result the new scheme reduces the numerical dissipation significantly and gives a more accurate representation of wave interactions. We extend the scheme to third order accuracy in one and two space dimensions. For third order accuracy we use central-WENO reconstruction, see Jiang & Shu [10], and Levy et al. [18, 19]. To improve temporal accuracy we use third order Runge-Kutta time stepping method. In the relativistic hydrodynamics the CFL condition is very simple. Every signal is bounded by the speed of light, therefore it is natural to take $\Delta t = 0.5 \min(\Delta x, \Delta y)$. Here Δt is the time step and Δx, Δy are the cell widths in the two-dimensional spatial domain.

There are mainly two kinds of flux functions derived from the inviscid Euler equations. The first group is the flux vector splitting (FVS) schemes. Flux splitting is a technique for achieving upwinding bias in numerical flux function, which is a natural consequence of regarding a fluid as an ensemble of particles. Since particles can move forward or backward, this automatically splits the fluxes of mass, momentum and energy into forward and backward fluxes through the cell interface, i.e.,

$$F_{i+\frac{1}{2}} = F^{+}(W_i) + F^{-}(W_{i+1}) \,,$$

where W_i represents mass, momentum and energy densities inside the cell i. The equivalence between the above splitting mechanism and the collisionless Boltzmann equation was first realized by Harten, Lax and van Leer [9]. Numerically it is observed that the explicit flux formulation of the KFVS schemes by solving the collisionless Boltzmann equation is identical to the flux function of van Leer [20]. We will discuss the KFVS scheme for the solution of SRHD equations. For more discussion on the KFVS schemes the reader is referred to Deshpande et al. [4, 5] and Xu et al. [35, 36, 37].

On the other hand, the FDS schemes based on the exact or approximate Riemann solvers, such as the Godunov, Roe and Osher methods [8, 26, 28], account for the wave interactions in the gas evolution process. Especially for the Godunov method, the exact Riemann solution of the Euler equations is used. The wave interaction in the FDS scheme can be clearly observed in the Roe's average $\overline{W}_{i+\frac{1}{2}}$ between the left W_i and the right state W_{i+1}. In the smooth flow region, there is basically no difference among the Godunov, Roe and Osher schemes. For example, the above three schemes can precisely keep a shear layer in the 2D case once the shear layer is aligned with the mesh. This fact is consistent with the exact solution of the Euler equations. Therefore, the FDS schemes can accurately capture the Navier-Stokes solutions in the resolved dissipative boundary layer, where the numerical dissipation is much smaller than the physical dissipation, see Xu [37] for details. However, this advantage is also accompanied with a disadvantage. The Godunov scheme in strong shock regions produces spurious oscillations such as the carbuncle phenomena and odd-even decoupling in the multi-dimensional case. KFVS schemes do not generate these spurious solutions, since they are intrinsically solving "viscous" equations rather than the inviscid Euler equations. An optimum choice to get a better scheme is to combine both, the KFVS and FDS methodology. The resulting method of this combination is be the so called BGK-type KFVS scheme which was extensively studied by Xu [36, 37] in the non-relativistic case. We will now generalize Xu's ideas to the SRHD case.

This paper consists of five sections. In Section 2, we give a brief introduction to relativistic kinetic theory. We give the relativistic kinetic phase density and its moments which recover all the constitutive relations of the SRHD equations. Furthermore, we reduce the three-dimensional moment intergrals to surface integrals over a unit sphere. In Section 3, we derive the kinetic flux splitting method for the SRHD equations in one and two space dimensions. We extend our scheme to third order by using a central-WENO initial reconstruction and a Runge-Kutta time stepping method. In Section 4, we give some numerical test computations in one and two space dimensions. In the one dimensional case, we compare our results with the solution of an exact Riemann solver of Martí and Müller [22, 23]. In Section 5, we give our conclusions on the results.

2 Special Relativistic Hydrodynamics

The coordinates with respect to a fixed reference frame are given by the 4-vector x^μ, $\mu \in \{0, 1, 2, 3\}$, where $x^0 = t$ is the observer time. The three vector $\mathbf{x} = x^i$, $i \in \{1, 2, 3\}$, denotes the spatial coordinates of any event x^μ. For simplicity we set $c = \hbar = k_B = 1$. Furthermore we assume that the metric tensor $g_{\mu\nu}$ is given by a diagonal matrix $g_{\mu\nu} = g^{\mu\nu} = \mathrm{diag}(1, -1, -1, -1)$.

The 4-momentum of the gas particles $q^\mu = (q^0, \mathbf{q})$ with $\mathbf{q} = q^i$, $i \in \{1, 2, 3\}$ is a kinetic variable. However, not all components of the 4-momentum are independent, because

$$q^\mu q_\mu = m^2, \tag{2.1}$$

where m is the rest mass of the particles. The invariant volume element $d\omega$ of the momentum space is given by

$$d\omega = \frac{1}{q^0} dq^1 dq^2 dq^3 = \frac{1}{q^0} d^3 q. \tag{2.2}$$

The phase density $f(x^\mu, q^m) \equiv f(t, \mathbf{x}, \mathbf{q})$ gives the number density of particles in the element $d\omega$ at x^μ.

Next we introduce the macroscopic 4-velocity u^μ by

$$u^\mu = \frac{1}{n} N^\mu, \quad \rho = \sqrt{N^\nu N_\nu}\,, \tag{2.3}$$

so that $u^\mu u_\mu = 1$, and ρ is a particle density. The fluid velocities v^i are given by

$$u^\mu = \gamma(1, v^i)\,, \quad \gamma = u^0 = \frac{1}{\sqrt{1-\mathbf{v}^2}}\,, \quad i = 1, 2, 3\,, \tag{2.4}$$

where γ is called the Lorentz factor.

Using the Einstein summation convention the equations describing the motion of a relativistic fluid are given by the five conservation laws

$$\partial_\mu N^\mu = 0, \quad \partial_\mu T^{\mu\nu} = 0\,. \tag{2.5}$$

Here N^μ is a particle density four-vector and $T^{\mu\nu}$ is energy momentum tensor. These tensors are given by

$$N^\mu = \rho u^\mu \quad \text{and} \quad T^{\mu\nu} = (e+p)u^\mu u^\nu - p g^{\mu\nu}\,, \tag{2.6}$$

where ρ is rest mass density, p is pressure and e is internal energy. In order to close the system we have the following relation for the energy density

$$e = \rho + \frac{p}{\Gamma - 1}\,, \tag{2.7}$$

where Γ is adiabatic index, and $\Gamma = \frac{5}{3}$ in the mildly relativistic case, while $\Gamma = \frac{4}{3}$ in the ultra-relativistic case. Also in the ultra-relativistic case the rest mass density in the (2.7) is zero hence we get $e = 3p$ in the ultra-relativistic case.

In oder to correctly recover the constitute relations (2.6), we have to modify the ultra-relativistic phase density and its moments, see our articles [14, 15]. This ultra-relativistic phase density was obtained from the Jüttner phase density [12] in the ultra-relativistic limit [14]. In the ultra-limit the rest mass is zero, i.e. $m = 0$, so that

$$q_0 \equiv |\mathbf{q}| \quad \text{and} \quad d\omega = \frac{d^3q}{|\mathbf{q}|}\,. \tag{2.8}$$

The aim is to modify the phase density and its moments in such a way that we recover all the constitutive relations (2.6), and still we can enjoy the simplicity of the phase density and its moments which we were able to obtain in the ultra-limit. The modified phase density is given by

$$\begin{aligned} f_J\left(\rho,\, T,\, \mathbf{u},\, \mathbf{q}\right) &= \frac{\rho\lambda^3}{8\pi}\, \exp\left(-\lambda u_\mu q^\mu\right) \\ &= \frac{\rho\lambda^3}{8\pi}\, \exp\left[-\lambda|\mathbf{q}|\gamma\left(1 - \mathbf{v}\cdot\frac{\mathbf{q}}{|\mathbf{q}|}\right)\right]. \end{aligned} \tag{2.9}$$

Here $\lambda = \dfrac{4\rho}{e+p}$ is the normalization factor. The only modification we made in the phase density is the change of the normalization factor λ. Since in the ultra case $e = 3p$, therefore we get back the normalization factor $\lambda = \frac{1}{T}$ in the ultra-limit, where T denotes the temperature which is defined by $T = p/\rho$.

Next we need to modify the moments of this phase density. We have the following modified moments of the above modified phase density

$$N^\mu = N^\mu(t,\mathbf{x}) = \int_3 q^\mu f(t,\mathbf{x},\mathbf{q})\,\frac{d^3q}{|\mathbf{q}|}\,, \tag{2.10}$$

$$T^{\mu\nu} = T^{\mu\nu}(t,\mathbf{x}) = \int_3 \left(q^\mu q^\nu + \delta g^{\mu\nu}\right) f(t,\mathbf{x},\mathbf{q})\,\frac{d^3q}{|\mathbf{q}|}, \tag{2.11}$$

where

$$\delta = \frac{e - 3p}{2\rho\lambda}. \tag{2.12}$$

The only modification is the additional term in th energy momentum tensor, i.e the term $\delta g^{\mu\nu}$. Again for the ultra-case this term is identically zero and we get back the moments for the ultra-case. Furthermore, the entropy four vector is given by

$$S^\mu = S^\mu(t,\mathbf{x}) = -\int_3 q^\mu f(t,\mathbf{x},\mathbf{q}) \ln\left(f(t,\mathbf{x},\mathbf{q})\right) \frac{d^3q}{|\mathbf{q}|}. \tag{2.13}$$

We can rewrite (2.5) in the following form

$$\frac{\partial \mathbf{W}}{\partial t} + \sum_{i=1}^{d} \frac{\partial F^i(\mathbf{W})}{\partial x^i} = 0\,, \tag{2.14}$$

where $\mathbf{W}$ is the vector of conserved variables and F^i are their corresponding fluxes along each direction, while d is the number of spatial dimensions. Equations (2.5) and(2.6) implies

$$\mathbf{W}(\mathbf{w}) = \left[\rho\gamma, (e+p)\gamma^2 v^i, (e+p)\gamma^2 - p\right]^T\,, \tag{2.15}$$

$$F^i(\mathbf{W}) = \left[\rho\gamma v^i, (e+p)\gamma^2 v^i v^j + p\delta^{ij}, (e+p)\gamma^2 v^i\right]^T\,, \tag{2.16}$$

where $\mathbf{w} = [\rho, v^j, p]$ are called primitive variables, and therefore the numerical techniques largely applied for Euler equations can also be applied to the relativistic Euler equations too. The above equations are strictly hyperbolic with corresponding eigenvalues (along each direction of spatial derivation):

$$\lambda_\pm = \frac{1}{1-\mathbf{v}^2 c_s^2}\left\{v_\|(1-c_s^2) \pm c_s\sqrt{(1-\mathbf{v}^2)[1-v_\|^2 - (\mathbf{v}^2 - v_\|^2)c_s^2]}\right\}\,, \quad \lambda = v_\|\,, \tag{2.17}$$

where the sound speed $c_s = \sqrt{\dfrac{\Gamma p}{(e+p)}}$. The equation $(2.17)_1$ simplifies to $\lambda_\pm = \dfrac{v \pm c_s}{1 \pm v c_s}$ in the one-dimensional case.

In any numerical time advancing routine, the primitive variables $\mathbf{w}$ have to be derived from the conservative ones at least once per time step. If we define

$$\mathbf{W} = \left[D, Q^i, E\right]\,,$$

where $D = \rho\gamma$, $Q^j = U v^j$, and $E = U - p$ with $U = (e+p)\gamma^2$. The system to be inverted can be cast in single equation for γ, cf. Del Zanna et al. [39]:

$$U(\gamma)^2\left(1-\gamma^{-2}\right) - \mathbf{Q}^2 = 0\,, \tag{2.18}$$

with $U = (e+p)\gamma^2 = D\gamma + \Gamma_1\gamma^2 p$, here $\Gamma_1 = \Gamma/(\Gamma-1)$, and $p = U - E$, so that

$$U(\gamma) = \frac{E\Gamma_1\gamma^2 - D\gamma}{\Gamma\gamma^2 - 1}\,. \tag{2.19}$$

Once we obtain γ, the variables ρ, p, $\mathbf{v}$ can be easily obtained from the above relations. Furthermore, we are able to obtain an important reduction of the moment integrals (2.10) and (2.11) which is presented in the Appendix A.

3 Kinetic Flux Splitting Method

In this section we derive the kinetic flux method in one and two space dimentions.

3.1 One-Dimensional Kinetic Flux Splitting Method

In gas-kinetic theory, the flux is associated with the particle motion across a cell interface. For 1D flow in the x-direction, the particle motion in this direction determines the flux function. Other quantities, such as density, thermal energy, and pressure can be considered as passive scalars which are transported with the x-direction particle velocity. Normally particles are randomly distributed around the average velocity. From statistical mechanics, the moving particles in the x-direction can be most favorably described by the relativistic Maxwellian (2.9), i.e. Jüttner phase density. For SRHD case we will use the same technique which was used by Xu [36] in the case of classical MHD equation.

The transport of any flow quantity is basically due to the movement of particles. With the phase density f_J in (2.9), we can split the particles into two groups. One group is moving to the right with $v_x > 0$ and the other group is moving to the left with $v_x < 0$. For the present one-dimensional variation of the SRHD equations it is sufficient to consider only the one-dimensional phase density. Before splitting the fluxes we introduce the new coordinates $-1 \leq \xi \leq 1,\ -\pi \leq \vartheta \leq \pi$

$$n^1 = \xi\,, \quad n^2 = \sqrt{1-\xi^2}\sin\vartheta\,, \quad n^3 = \sqrt{1-\xi^2}\cos\vartheta\,. \tag{3.1}$$

Introducing these new coordinates in (A-2)$_1$ and (A-3) we get after canceling the density $\rho(t,x)$ on both sides of the equality

$$\langle u^0\rangle = 1 = \int_{-1}^{1} \frac{1}{2\gamma^2(1-\xi v_x)^2} d\xi\,, \quad \langle u^1\rangle = v_x = \int_{-1}^{1} \frac{\xi}{2\gamma^3(1-\xi v_x)^3} d\xi\,. \tag{3.2}$$

The above two moments are sufficient to split all the fluxes. Also we can see that the normalization factor drops out completely and we get the moments which are only depending on the macroscopic velocity v_x. This is the main reason behind the use of ultra-relativistic phase density as the velocity repartition function in this case for SRHD equations. In order to simplify the notation we define

$$\langle u^0\rangle_+ = \int_{0}^{1} \frac{1}{2\gamma^2(1-\xi v_x)^2} d\xi\,, \quad \langle u^0\rangle_- = \int_{-1}^{0} \frac{1}{2\gamma^2(1-\xi v_x)^2} d\xi\,. \tag{3.3}$$

Similarly

$$\langle u^1\rangle_+ = \int_{0}^{1} \frac{\xi}{2\gamma^3(1-\xi v_x)^3} d\xi\,, \quad \langle u^1\rangle_- = \int_{-1}^{0} \frac{\xi}{2\gamma^3(1-\xi v_x)^3} d\xi\,. \tag{3.4}$$

The above integrals gives

$$\langle u^0 \rangle_\pm = \frac{1}{2}\left(1 \pm v_x\right) \ , \quad \langle u^1 \rangle_\pm = \pm\frac{1}{4}\left(1 \pm v_x\right)^2 \ . \tag{3.5}$$

After having the above definitions, we are ready to split the 1D form of SRHD flux function (2.16),

$$F = \begin{pmatrix} \rho\gamma v_x \\ (e+p)\gamma^2 v_x^2 + p \\ (e+p)\gamma^2 v_x \end{pmatrix} = F_f^+ + F_f^- \ , \tag{3.6}$$

where

$$F_f^\pm = \langle u^1 \rangle_\pm \begin{pmatrix} \rho\gamma \\ (e+p)\gamma^2 v_x \\ (e+p)\gamma^2 \end{pmatrix} + \langle u^0 \rangle_\pm \begin{pmatrix} 0 \\ p \\ 0 \end{pmatrix} . \tag{3.7}$$

When we conclude the above splitting of fluxes, the free transport flux for the SRHD equations at a cell interface becomes

$$F^f_{i+\frac{1}{2}} = F^+_{i,f} + F^-_{i+1,f} \ , \tag{3.8}$$

where "f" is used to denote the above free transport model. The KFVS-type method is very robust, but over diffusive, especially in the case with the coarse mesh. To reduce numerical dissipation, Xu [36] in classical MHD case implemented a particle collision mechanism in above flux transporting process. Also we have used a similar method in order to derive the BGK-type KFVS scheme for the ultra-relativistic Euler equations [16]. The idea is to obtain an equilibrium state $\overline{W}_{i+\frac{1}{2}}$ at the cell interface by combining the left and right moving beams and use this state to get an equilibrium flux function $F^e(\overline{W}_{i+\frac{1}{2}})$ through the flux function definition in (3.6). Using (2.15), the equilibrium state at the cell interface can be obtained as

$$\overline{W}_{i+\frac{1}{2}} = \begin{pmatrix} \rho\gamma \\ (e+p)\gamma^2 v_x \\ (e+p)\gamma^2 - p \end{pmatrix} = W_i^+ + W_{i+1}^- \ , \tag{3.9}$$

where

$$W_i^\pm = \begin{pmatrix} \rho\gamma \langle u^0 \rangle_\pm \\ (e+p)\gamma^2 \langle u^1 \rangle_\pm \\ \left[(e+p)\gamma^2 - p\right] \langle u^0 \rangle_\pm \end{pmatrix}_i \ . \tag{3.10}$$

With the above averaged macroscopic variables $\overline{W}_{i+\frac{1}{2}}$, the equilibrium flux can be obtained as

$$F^e_{i+\frac{1}{2}} = F^e(\overline{W}_{i+\frac{1}{2}}) = \begin{pmatrix} \overline{\rho}\,\overline{\gamma}\,\overline{v}_x \\ (\overline{e}+\overline{p})\overline{\gamma}^2 \overline{v}_x^2 + \overline{p} \\ (\overline{e}+\overline{p})\overline{\gamma}^2 \overline{v}_x \end{pmatrix} . \tag{3.11}$$

The final flux function is a combinaion of non-equilibrium and equilibrium flux functions

$$F_{i+\frac{1}{2}} = \chi F^f_{i+\frac{1}{2}} + (1-\chi) F^e_{i+\frac{1}{2}}\,, \tag{3.12}$$

where χ is an adaptive parameter, see [36]. In the first order scheme χ can be fixed, say, 0.7 or 0.5, in the numerical calculations. Theoretically χ should depend on the real flow situations: in equilibrium and smooth regions, the use of $\chi \sim 0$ is physically reasonable, and in the regions with discontinuities, χ should be close to 1 in order to have enough numerical dissipation to recover smooth shock transition. A possible choice for η in high order scheme is to consider it as a function of the pressure difference, such as the switch function in the JST scheme [11], see Xu [36] for further details.

In 1D case the integration of the (2.14) over the cell $I_i = \left[x_{i-\frac{1}{2}}, x_{i+\frac{1}{2}}\right]$ gives the following semi-discrete kinetic upwind scheme

$$\frac{dW_i}{dt} = -\frac{F_{i+\frac{1}{2}} - F_{i-\frac{1}{2}}}{\Delta x}. \tag{3.13}$$

where $F_{i+\frac{1}{2}}$ is the fluxes at the cell boundary $x_{i+\frac{1}{2}}$ and is given by (3.12). Here Δx represent the cell width. The above scheme is only first order accurate in space. To get high order accuracy, the initial reconstruction strategy must be applied to interpolate the cell averaged variables W_i^n.

Third-Order Accuracy

For the third-order accuracy we use the central-WENO (CWENO) reconstruction which was recently presented in Levy [19] as well as Kurganov & Levy [18]. We apply this reconstruction to the primitive variables $\mathbf{w} = [\rho, v, p]$. This was found to be more suitable in relativistic flows, see [39]. Here we give a brief overview of the method.

In each cell I_i we reconstruct a quadratic polynomial as a convex combination of three polynomials $P_L(x)$, $P_R(x)$, and $P_C(x)$,

$$P_i(x) = \lambda_L P_L(x) + \lambda_R P_R(x) + \lambda_C P_C(x)\,, \tag{3.14}$$

with positive weights $\lambda_i \geq 0\ \forall_i \in \{C, R, L\}$ and $\sum_i \lambda_i = 1$. The polynomials $P_L(x)$, $P_R(x)$ correspond to left and right one-sided linear reconstructions, respectively, while $P_C(x)$ is a parabola, centered around x_i.

The linear functions, $P_R(x)$ and $P_L(x)$ are uniquely determined by requiring them to conserve the one-sided cell averages (w_i^n, w_{i+1}^n and w_i^n, w_{i-1}^n, respectively) as

$$P_R(x) = w_i^n + \frac{w_{i+1}^n - w_i^n}{\Delta x}(x - x_i)\,, \quad P_L(x) = w_i^n + \frac{w_i^n - w_{i-1}^n}{\Delta x}(x - x_i)\,. \tag{3.15}$$

The centered parabola, P_C, is chosen so as to satisfy

$$P_{EXACT}(x) = c_L P_L(x) + c_R P_R(x) + (1 - c_L - c_R) P_C(x)\,, \tag{3.16}$$

with constants c_i's.

Let the approximations to the point-values of $w(x_i, t^n)$, $w_x(x_i, t^n)$, and $w_{xx}(x_i, t^n)$ be denoted by w_i, w_i', w_i''. They are are given as

$$
\begin{aligned}
w_i &= w_i^n - \frac{1}{24}(w_{i+1}^n - 2w_i^n + w_{i-1}^n)\,, \\
w_i' &= \frac{w_{i+1}^n - w_{i-1}^n}{2\Delta x}\,, \quad w_i'' = \frac{w_{i-1}^n - 2w_i^n + w_{i+1}^n}{\Delta x^2}\,.
\end{aligned}
\tag{3.17}
$$

Then $P_{EXACT}(x)$ is the unique parabola that conserves the three cell averages, w_{i-1}^n, w_i^n, and w_{i+1}^n, which is given by

$$
P_{EXACT}(x) = w_i + w_i'(x - x_i) + \frac{1}{2}w_i''(x - x_i)^2\,. \tag{3.18}
$$

In [19] it was shown that every symmetric selection of the constants c_i's in (3.16) will provide the desired third-order accuracy. For example, by taking $c_L = c_R = \frac{1}{4}$, (3.15)-(3.18) yields

$$
\begin{aligned}
P_C(x) =& w_i^n - \frac{1}{12}(w_{i+1}^n - 2w_i^n + w_{i-1}^n)\,, \\
&+ \frac{w_{i+1}^n - w_{i-1}^n}{2\Delta x}(x - x_i) + \frac{w_{i-1}^n - 2w_i^n + w_{i+1}^n}{\Delta x^2}(x - x_i)^2\,.
\end{aligned}
\tag{3.19}
$$

In smooth regions, the coefficients λ_i of the convex combination in (3.14) are chosen to guarantee the maximum order of accuracy, in this particular case order three. But in the presence of a discontinuity they are automatically switched to the best one-sided stencil, which generates the least oscillatory reconstruction. The weights are taken as

$$
\lambda_j = \frac{\alpha_j}{\sum_m \alpha_m}\,, \text{ where } \alpha_j = \frac{c_j}{(\epsilon + IS_j)^p}\,, \quad j, m \in \{C, R, L\}\,, \tag{3.20}
$$

$$
c_L = c_R = 1/4\,,\ c_C = 1/2\,. \tag{3.21}
$$

The constant ϵ guarantees that the denominator does not vanish and is taken as $\epsilon = 10^{-6}$. The value of p may be chosen to provide the highest accuracy in smooth areas and to ensure the nonoscillatory nature of the solution near the discontinuities, consult [10]. In [10] the value of $p = 2$ was empirically selected, and here we use the same value of p. Finally the smoothness indicator, IS_i, are defined as

$$
IS_j = \sum_{l=1}^{2} \int_{x_{i-1/2}}^{x_{i+1/2}} (\Delta x)^{2l-1} \left(P_j^{(l)}(x)\right)^2 dx\,. \tag{3.22}
$$

A direct computation then results in

$$
\begin{aligned}
IS_L &= (w_i^n - w_{i-1}^n)^2\,, \quad IS_R = (w_{i+1}^n - w_i^n)^2\,, \\
IS_C &= \frac{13}{3}(w_{i+1}^n - 2w_i^n + w_{i-1}^n)^2 + \frac{1}{4}(w_{i+1}^n - w_{i-1}^n)^2\,.
\end{aligned}
\tag{3.23}
$$

It is easy to see that in the presence of large gradients, this reconstruction switches to one of the second order one sided linear reconstructions, P_R or P_L. For more details we refer the reader to [19].

In this case the values of w_i at the extreme points $x_{i-\frac{1}{2}}$ and $x_{i+\frac{1}{2}}$ are

$$w_i^L = A_i - \frac{\Delta x}{2} B_i + \frac{(\Delta x)^2}{8} C_i \,, \tag{3.24}$$

$$w_i^R = A_i + \frac{\Delta x}{2} B_i + \frac{(\Delta x)^2}{8} C_i \,, \tag{3.25}$$

where

$$A_i = W_i^n - \frac{\lambda_C}{12}(w_{i+1}^n - 2w_i^n + w_{i-1}^n) \,, \tag{3.26}$$

$$B_i = \frac{1}{\Delta x}\left[\lambda_R(w_{i+1}^n - w_i^n) + \lambda_C \frac{w_{i+1}^n - w_{i-1}^n}{2} + \lambda_L(w_i^n - w_{i-1}^n)\right] \,, \tag{3.27}$$

$$C_i = 2\lambda_C \frac{w_{i+1}^n - 2w_i^n + w_{i-1}^n}{\Delta x^2} \,, \tag{3.28}$$

where λ_L, λ_C and λ_R are defined by (3.20). Based on the above reconstruction, the high spatial resolution kinetic SRHD solver becomes

$$\frac{dW_i}{dt} = -\frac{F_{i+\frac{1}{2}}(w_{i+1}^L, w_i^R) - F_{i-\frac{1}{2}}(w_i^L, w_{i-1}^R)}{\Delta x} \,, \tag{3.29}$$

where the W_i are conserved variables and w_i^L, w_i^R are the extreme values of the reconstructed primitive variables which are given by (3.24) and (3.25).

To improve the temporal accuracy, we use a third-order TVD Runge-Kutta scheme to solve (3.29). Denoting the right-hand side of (3.29) as $L(W)$, the third-order TVD Runge-Kutta scheme updates W through the following three stages:

$$\begin{aligned} W^{(1)} &= W^n + \Delta t L(W^n) \,, \\ W^{(2)} &= \frac{3}{4}W^n + \frac{1}{4}\left(W^{(1)} + \Delta L(W^{(1)})\right) \,, \\ W^{n+1} &= \frac{1}{3}W^n + \frac{2}{3}\left(W^{(2)} + \Delta L(W^{(2)})\right) \,. \end{aligned} \tag{3.30}$$

3.2 Two-Dimensional Kinetic Flux Splitting Method

In this subsection we extend the one-dimensional gas-kinetic flux splitting method to the two-dimensional case. The method follows the same lines as in the 1D case. With the phase density f_J in (2.9), we can split the particles into four groups. One group is moving to the right with $v_x > 0$, the second group is moving to the left with $v_x < 0$, the third group is moving upward with $v_y > 0$, and the fourth group is moving downward with $v_y < 0$. For the present two-dimensional variation of the SRHD equations it is sufficient to consider the two-dimensional form of the phase density. Before splitting the fluxes we again introduce the new coordinates (3.1). Introducing these new coordinates in $(A\text{-}2)_1$ and (A-3) we get in the two-dimensional case

$$\begin{aligned}
\langle u^0\rangle = 1 &= \frac{1}{4\pi}\int_{-\pi}^{\pi}\int_{-1}^{1}\frac{1}{\gamma^2(1-\xi v_x-\sqrt{1-\xi^2}\sin\vartheta v_y)^2}d\xi d\vartheta\,, \\
\langle u^1\rangle_x = v_x &= \frac{1}{4\pi}\int_{-\pi}^{\pi}\int_{-1}^{1}\frac{\xi}{\gamma^4(1-\xi v_x-\sqrt{1-\xi^2}\sin\vartheta v_y)^3}d\xi d\vartheta\,, \qquad (3.31)\\
\langle u^1\rangle_y = v_y &= \frac{1}{4\pi}\int_{-\pi}^{\pi}\int_{-1}^{1}\frac{\sqrt{1-\xi^2}\sin\vartheta}{\gamma^4(1-\xi v_x-\sqrt{1-\xi^2}\sin\vartheta v_y)^3}d\xi d\vartheta\,.
\end{aligned}$$

The above three moments are sufficient to split all the fluxes. Also we can see that the normalization factor drops out completely and we get the moments which are only depending on the macroscopic velocities v_x and v_y. In order to simplify the notation we define

$$\langle u^0\rangle_{+x} = \frac{1}{4\pi}\int_{-\pi}^{\pi}\int_{0}^{1}\frac{1}{\gamma^2(1-\xi v_x-\sqrt{1-\xi^2}\sin\vartheta v_y)^2}d\xi d\vartheta\,, \qquad (3.32)$$

$$\langle u^0\rangle_{-x} = \frac{1}{4\pi}\int_{-\pi}^{\pi}\int_{-1}^{0}\frac{1}{\gamma^2(1-\xi v_x-\sqrt{1-\xi^2}\sin\vartheta v_y)^2}d\xi d\vartheta\,. \qquad (3.33)$$

Similarly we can split the other moments. In summary we get the following moments

$$\langle u^0\rangle_{\pm x} = \frac{1}{2}\left(1\pm\frac{v_x}{\sqrt{1-v_y^2}}\right)\,, \quad \langle u^0\rangle_{\pm y} = \frac{1}{2}\left(1\pm\frac{v_y}{\sqrt{1-v_x^2}}\right)\,, \qquad (3.34)$$

$$\langle u^1\rangle_{\pm x} = \frac{v_x}{2}\pm\frac{1+v_x^2-v_y^2}{4\sqrt{1-v_y^2}}\,, \quad \langle u^1\rangle_{\pm y} = \frac{v_y}{2}\pm\frac{1+v_y^2-v_x^2}{4\sqrt{1-v_x^2}}\,. \qquad (3.35)$$

After having the above definitions, we are ready to split the 2D form of SRHD flux functions (2.16),

$$F = \begin{pmatrix} \rho\gamma v_x \\ (e+p)\gamma^2 v_x^2 + p \\ (e+p)\gamma^2 v_x v_y \\ (e+p)\gamma^2 v_x \end{pmatrix} = F_f^+ + F_f^-\,, \qquad (3.36)$$

where

$$F_f^{\pm} = \langle u^1\rangle_{\pm x}\begin{pmatrix} \rho\gamma \\ (e+p)\gamma^2 v_x \\ (e+p)\gamma^2 v_y \\ (e+p)\gamma^2 \end{pmatrix} + \langle u^0\rangle_{\pm x}\begin{pmatrix} 0 \\ p \\ 0 \\ 0 \end{pmatrix}\,, \qquad (3.37)$$

and

$$G = \begin{pmatrix} \rho\gamma v_y \\ (e+p)\gamma^2 v_x v_y \\ (e+p)\gamma^2 v_y^2 + p \\ (e+p)\gamma^2 v_y \end{pmatrix} = G_f^+ + G_f^- \,, \tag{3.38}$$

where

$$G_f^{\pm} = \langle u^1 \rangle_{\pm y} \begin{pmatrix} \rho\gamma \\ (e+p)\gamma^2 v_x \\ (e+p)\gamma^2 v_y \\ (e+p)\gamma^2 \end{pmatrix} + \langle u^0 \rangle_{\pm y} \begin{pmatrix} 0 \\ 0 \\ p \\ 0 \end{pmatrix} . \tag{3.39}$$

When we conclude the above splitting of fluxes, the free transport flux for the SRHD equations at a cell interface become

$$F^f_{i+\frac{1}{2}} = F^+_{i,j,f} + F^-_{i+1,j,f} \,, \quad G^f_{i+\frac{1}{2},j} = G^+_{i,j,f} + G^-_{i,j+1,f} \,. \tag{3.40}$$

To obtain an equilibrium states $\overline{W}_{i+\frac{1}{2},j}$ and $\overline{W}_{i,j+\frac{1}{2}}$ at the cell interfaces we have

$$\overline{W}_{i+\frac{1}{2},j} = \begin{pmatrix} \rho\gamma \\ (e+p)\gamma^2 v_x \\ (e+p)\gamma^2 v_y \\ (e+p)\gamma^2 - p \end{pmatrix}_{i+\frac{1}{2},j} = W^+_{i,j} + W^-_{i+1,j} \,, \tag{3.41}$$

where

$$W^{\pm}_{i,j} = \begin{pmatrix} \rho\gamma \langle u^0 \rangle_{\pm x} \\ (e+p)\gamma^2 \langle u^1 \rangle_{\pm x} \\ (e+p)\gamma^2 v_y \langle u^0 \rangle_{\pm x} \\ \left[(e+p)\gamma^2 - p\right] \langle u^0 \rangle_{\pm x} \end{pmatrix}_{i,j} . \tag{3.42}$$

Similarly

$$\overline{W}_{i,j+\frac{1}{2}} = \begin{pmatrix} \rho\gamma \\ (e+p)\gamma^2 v_x \\ (e+p)\gamma^2 v_y \\ (e+p)\gamma^2 - p \end{pmatrix}_{i,j+\frac{1}{2}} = W^+_{i,j} + W^-_{i,j+1} \,, \tag{3.43}$$

where

$$W^{\pm}_{i,j} = \begin{pmatrix} \rho\gamma \langle u^0 \rangle_{\pm y} \\ (e+p)\gamma^2 \langle u^1 \rangle_{\pm y} \\ (e+p)\gamma^2 v_y \langle u^0 \rangle_{\pm y} \\ \left[(e+p)\gamma^2 - p\right] \langle u^0 \rangle_{\pm y} \end{pmatrix}_{i,j} . \tag{3.44}$$

With the above averaged macroscopic variables $\overline{W}_{i+\frac{1}{2},j}$ and $\overline{W}_{i,j+\frac{1}{2}}$, the equilibrium fluxes can be obtained as

$$F^e_{i+\frac{1}{2},j} = F^e(\overline{W}_{i+\frac{1}{2},j}) = \begin{pmatrix} \overline{\rho}\,\overline{\gamma}\,\overline{v}_x \\ (\overline{e}+\overline{p})\overline{\gamma}^2\overline{v}_x^2 + \overline{p} \\ (\overline{e}+\overline{p})\overline{\gamma}^2\overline{v}_x\overline{v}_y \\ (\overline{e}+\overline{p})\overline{\gamma}^2\overline{v}_x \end{pmatrix}, \tag{3.45}$$

and

$$G^e_{i,j+\frac{1}{2}} = F^e(\overline{W}_{i,j+\frac{1}{2}}) = \begin{pmatrix} \overline{\rho}\,\overline{\gamma}\,\overline{v}_y \\ (\overline{e}+\overline{p})\overline{\gamma}^2\overline{v}_x\overline{v}_y \\ (\overline{e}+\overline{p})\overline{\gamma}^2\overline{v}_x^2 + \overline{p} \\ (\overline{e}+\overline{p})\overline{\gamma}^2\overline{v}_y \end{pmatrix}. \tag{3.46}$$

The final flux function is a combinaion of non-equilibrium and equilibrium flux functions

$$F_{i+\frac{1}{2},j} = \chi F^f_{i+\frac{1}{2},j} + (1-\chi)F^e_{i+\frac{1}{2},j}\,, \tag{3.47}$$

$$G_{i,j+\frac{1}{2}} = \chi G^f_{i,j+\frac{1}{2}} + (1-\chi)F^e_{i,j+\frac{1}{2}}\,. \tag{3.48}$$

where χ is again an adaptive parameter, see [36].

In 2D case the integration of the (2.14) over the cell $I_{i,j} = \left[x_{i-\frac{1}{2}}, x_{i+\frac{1}{2}}\right] \times \left[y_{j-\frac{1}{2}}, y_{j+\frac{1}{2}}\right]$ give the following semi-discrete kinetic upwind scheme

$$\frac{dW_i}{dt} = -\frac{F_{i+\frac{1}{2},} - F_{i-\frac{1}{2},j}}{\Delta x} - \frac{G_{i,j+\frac{1}{2}} - G_{i,j-\frac{1}{2}}}{\Delta y}\,, \tag{3.49}$$

where $F_{i+\frac{1}{2},j}$ and $G_{i,j+\frac{1}{2}}$ are the fluxes at the cell boundaries and is given by (3.47) and (3.48). Here Δx and Δy represent the cell widths in $x-$ and $y-$directions. The above scheme is only first order accurate in space and time. To get high order accuracy, the initial reconstruction strategy must be applied to interpolate the cell averaged primitive variables $w^n_{i,j}$. The third order CWENO reconstructions presented in the 1D case can be used direction by direction in order to reconstruct the intermediate values $w^n_{i+\frac{1}{2},j}$ and $w^n_{i,j+\frac{1}{2}}$. In the 2D case the only change will be an additional term in P_C of (3.19). The terms P_L and P_R are the same as in (3.15). In 2D the P_C is given by

$$\begin{aligned} P_C(x) = {} & w^n_{i,j} - \frac{1}{12}(w^n_{i+1,j} - 2w^n_{i,j} + w^n_{i-1,j})\,, \\ & - \frac{1}{12}(w^n_{i,j+1} - 2w^n_{i,j} + w^n_{i,j-1}) + \frac{w^n_{i+1,j} - w^n_{i-1,j}}{2\Delta x}(x - x_i) \\ & + \frac{w^n_{i-1,j} - 2w^n_{i,j} + w^n_{i+1,j}}{\Delta x^2}(x - x_i)^2\,. \end{aligned} \tag{3.50}$$

Note that the only difference between this formula and (3.19) is an additional term in the second line. This corresponds to the second derivative in the y direction and guarantees the third order accuracy of the computed extreme values at the cell boundaries. This "dimension by dimension" approach is implemented in our work.

To improve temporal accuracy, we again use the TVD Runge-Kutta method (3.30).

4 Numerical Case Studies

In this section the proposed scheme is validated against typical tests cases available in the current literature. We present one- and two-dimensional test cases here. All the simulations presented here use, unless explicitly specified, the classical value $\Gamma = 5/3$ for the adiabatic index. In all the results, unless specified, we have taken the adaptive parameter $\chi = 0.5$.

4.1 One-Dimensional Tests

Here we apply our kinetic scheme to reproduce the discontinuous profiles involved in the so called shock-tube problems. Given a unitary numerical 1D pipe of N grid points, two constant states (ρ, v, p) are taken on the left $(0 < x \leq 0.5)$ and on the right $(0.5 < x \leq 1)$ with respect to a diaphragm, placed initially at $x = 0.5$ and then removed. Typical patterns seen in the subsequent evolution are shocks, contact discontinuities and rarefaction waves. In the relativistic regime these features are qualitatively unchanged, since the structure of the characteristics is the same, but density jumps are not limited by any function of the adiabatic index and rarefaction waves do not yield straight profiles, due to the nonlinear Lorentz transformation formulae. We compare our numerical results with the results of the exact Riemann solver of [22, 23]. In all numerical computation we have used a natural CFL condition $\Delta t = \Delta x/2$, as every signal is bounded by the speed of light.

Problem 1: Shock tube problem I

The initial data are

$$(\rho, v, p)^L = (10.0, 0.0, 13.33)\,,$$
$$(\rho, v, p)^R = (1.0, 0.0, 0.66 \times 10^{-6}).$$

The spatial domain is taken as $[0, 1]$ with 400 mesh elements and the final time is $t = 0.4$. This problem involves the formation of an intermediate state bounded by a shock wave propagating to the right and a transonic rarefaction wave propagating to the left. The fluid in the intermediate state moves at a mildly relativistic speed $(v = 0.72c)$ to the right. Flow particles accumulate in a dense shell behind the shock wave compressing the fluid and heating it. The fluid is extremely relativistic from a thermodynamic point of view, but only mildly relativistic dynamically. Figure 2_a show the results.

Problem 2: Shock tube problem II

The initial data are

$$(\rho, v, p)^L = (1.0, 0.0, 1000)\,,$$
$$(\rho, v, p)^R = (1.0, 0.0, 0.01).$$

The spatial domain is taken as $[0, 1]$ with 500 mesh elements and the final time is $t = 0.35$. The flow pattern is similar to that of Problem 1, but more extreme. Relativistic effects reduce the post-shock state to a thin dense shell with width of only about 1% of the grid length at $t = 0.35$. The fluid velocity is $v = 0.96c$. The jump in the density is 10.6 for the exact Riemann solution while 7.2 in the case of the kinetic solution. The same height, i.e., 7.2 was observed by [39] from the solution of third order HHL and LLF schemes. The results are given in Figure 2_b.

Problem 3: Perturbed relativistic shock tube flow

This problem was considered by [38, 39]. The initial conditions are specified as $(\rho, v, p)^L = (5, 0, 50)$ for $0 \leq x \leq 0.5$ and $(\rho, v, p)^R = (\rho_R, 0, 5)$ for $0.5 \leq x \leq 1.0$. Here the right state is a perturbed density field of a sinusoidal wave, $\rho_R = 2 + 0.3\, \sin(50x)$. We run this test for 400 mesh points. The computed solutions are plotted at $t = 0.35$. The results for particle density ρ, velocity v and pressure p are shown in Figure 3. The exact solution is obtained by using our kinetic method on very fine mesh.

Problem 4: Two interacting relativistic blast waves

The initial data are

$$(n, u, p) = \begin{cases} (1, 0, 1000) & \text{if } 0 < x < 0.1\,, \\ (1, 0, 0.01) & \text{if } 0.1 < x < 0.9\,, \\ (1, 0, 100) & \text{if } 0.9 < x < 1.0\,, \end{cases}$$

where the computational domain is $0 \leq x \leq 1$. The collision of two strong blast waves was used by Woodward and Colella [34] to compare the performance of several numerical method in classical hydrodynamics. In the relativistic case, Yang et al. [38] considered this problem to test the high-order extensions of relativistic beam scheme, while Martí and Müller [22] used it to evaluate the performance of their relativistic PPM code. In this last case, the original boundary conditions were changed, from reflecting to outflow, to avoid the reflection and subsequent interaction of rarefaction waves allowing for a comparison with an analytical solution. We will also consider the outflow boundary conditions in this example. The results are given in Figure 4 for the particle density ρ, velocity v and pressure p. The number of mesh points are 600 and the output time is $t = 0.43$. We take the adiabatic index $\Gamma = 1.4$, which is the same as in the above cited articles. The exact solution is obtained by using our kinetic method on very fine mesh.

4.2 Two-Dimensional Tests

The multidimensional relativistic flow simulations are more difficult as compared to the one-dimensional case. The reason of this complexity is that the velocity components are interpolated separately, possibly failing the condition $\mathbf{v}^2 < 1$ in the ultra-relativistic regimes due to numerical errors in the reconstruction. For this reason in some cases we had to reduce to a first order reconstruction, namely when the Lorentz factor reaches $\gamma = 10$. Note that this does not mean in any sense that this threshold cannot be exceeded, but only to reduce accuracy in those regions, which usually are located at shock fronts where the order would have been lowered anyway. In all numerical computations we have used a natural CFL condition $\Delta t = 0.5 \min(\Delta x, \Delta y)$, as every signal is bounded by the speed of light.

Problem 5: Diffracting shock waves and the forward facing step

In this example we consider the shock diffraction at a corner. This is a relativistic analog of the classical experimental results presented by van Dyke [32]. Here the dimensions of the square region are less than those presented in [32]. The initial data are given in Figure 1 where a shock wave is standing at $x = 0.0$. The results are shown in Figure 5. A rolled-up vortex is generated at the corner. We have used 300×300 mesh points with a final time $t = 1.7$.

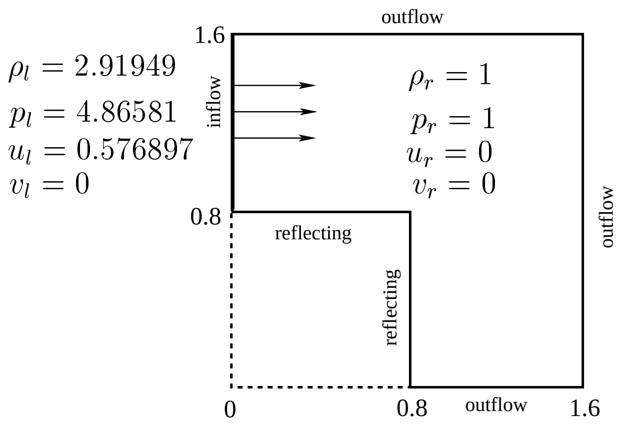

Figure 1: Initial data

Problem 6: Here we consider a two-dimensional version of shock tub problem, see [39]. We consider a square domain of side length 1. We divide this domain into four quadrants. The initial data are

$$
\begin{aligned}
(\rho, v_x, v_y, p)^{NE} &= (0.1, 0, 0, 0.01)\,,\\
(\rho, v_x, v_y, p)^{NW} &= (0.1, 0.99, 0, 1)\,,\\
(\rho, v_x, v_y, p)^{SW} &= (0.5, 0, 0, 1)\,,\\
(\rho, v_x, v_y, p)^{SE} &= (0.1, 0, 0.99, 1)\,.
\end{aligned}
$$

In this problem the four boundaries define two contact discontinuities and two 1D shocks, symmetric with respect to the main diagonal. Note that we have not taken an exact 1D shock across the N and E interfaces, and this may be recognized by observing the evolved discontinuities in Figure 6, converging toward the NE corner with their complete Riemann fan. In the rest of the domain the structure evolves with curved shock fronts and a complicated pattern in the SW quadrant, reminiscent of an oblique jet with bow shock and converging internal shock fronts. The lines in the SW direction with respect to the bow shock are actually due to spurious waves created at the W and S interfaces by the numerical diffusion term in the energy equation, left and right states have jump in kinetic energy, and cannot be removed even with a Roe-type solver. Note that we have used the diffusive form of our kinetic method, ie. $\eta = 0.7$, since for $\eta < 0.7$ the solution is unstable at the same high resolution.

Problem 7:

The next example considered here is the astrophysical relativistic jet problem. We simulate the propagation of an axisymmetric jet in 2D cylindrical coordinates (z, r). The domain is $0 < r < 14$ and $0 < z < 20$, with extrapolation boundaries, except at $z = 0$ within the jet radius where initial values are kept constant. At $t = 0$ a relativistic jet with $v_z = 0.99$ and density 100 times less than the surrounding, but same pressure, is located at $7 \leq r \leq 9$ and $z \leq 1$ as follows

$$
\begin{aligned}
(\rho, v_z, v_r, p)^{NE} &= (0.1, 0.99, 0, 0.01)\,, \quad 8 \leq r \leq 10\,,\; z \leq 1 \\
(\rho, v_z, v_r, p)^{NW} &= (10, 0, 0, 0.01)\,, \quad \text{outside.}
\end{aligned}
$$

The results are shown in Figure 7.

Problem 8: Explosion in a box

In this example we consider a two-dimensional Riemann problem inside a square box of sides length 1, with reflecting walls. Initially the velocities are zero and density is unity. The pressure is 10 inside a small square box of sides length 0.2 in the center of the large box, while pressure is 0.01 elsewhere. The results are shown at $t = 1.0$ and $t = 2.0$ in Figures 8, 9. In all the results we have used 400×400 mesh points.

5 Conclusions

In this paper we have derived a gas kinetic flux splitting method for the special relativistic Euler equations. The flux function is constructed with consideration of particle transport across the cell interface. Particle "collisions" are implemented in the transport process to reduce the numerical dissipation. The parameter χ, which determines the weights between the free transport and equilibrium fluxes takes constant values in the current study.

It is quite often that the requirement for robustness and accuracy in the design of a numerical scheme are in conflict with each other. If a scheme is robust, it is unnecessarily diffusive and if a scheme is accurate, it loses robustness. In order to get a correct representation of the flow motion in the discretized space and time, a consistent dissipative mechanism must be added in the gas evolution stage. An optimum choice is to take a combination of both free-flights and collisions. In shock regions we need more dissipation for smooth transition of shock while at the contact discontinuity we need more collisions, equilibrium case, to get a good resolution of the contact discontinuity. In this paper we have used a convex combination of the collisionless and collisional fluxes with χ as adaptive parameter.

We have modified the normalization factor of the ultra-relativistic phase density as well as its moments in order to correctly recover all the constitutive relations of the special relativistic hydrodynamic (SRHD) equations considered in this paper. In order to achieve third order accuracy of the scheme, we have used a third order central-WENO reconstruction in space, and a third order TVD Runge-Kutta time stepping method for the time derivatives. The results from the test cases show that this procedure worked well.

Although we have restricted our attention to one- and two-dimensional cases in the current paper, the extension of the current method to three space dimensions is straightforward.

Appendix A: Reduction of the Volume Integrals

Here we apply an important simplification to the volume integrals (2.10) and (2.11). We can see in (2.9) that the fields $\rho(t,\mathbf{x})$, $p(t,\mathbf{x})$, $e(t,\mathbf{x})$ and $\mathbf{v}(t,\mathbf{x})$ are not depending on $|\mathbf{q}|$. This fact enables us to reduce the three-fold volume integrals to two-fold surface integrals by applying polar coordinates, see [14, 16] for more details. Now using the relation

$$\int_{\mathbb{R}^3} f(|\mathbf{q}|)d^3q = \oint\limits_{\partial B(0,1)} \int\limits_0^\infty r^2 f(r)dr\,, \tag{A-1}$$

one get the following reduced surface integrals from the volume moment integrals (2.10) and (2.11). For abbreviation we introduce the unit vector $\mathbf{n} = \frac{\mathbf{q}}{|\mathbf{q}|}$, then we have

$$\begin{aligned} N^\mu(t,\mathbf{x}) &= \frac{1}{4\pi} \oint\limits_{\partial B(0,1)} \frac{n^\mu \rho(t,\mathbf{x})}{\gamma^3(1-\mathbf{n}\cdot\mathbf{v}(t,\mathbf{x}))^3}\, dS(\mathbf{n})\,, \\ T^{\mu\nu}(t,\mathbf{x}) &= \frac{3}{4\pi} \oint\limits_{\partial B(0,1)} \left(\frac{n^\mu n^\nu (e+p)(t,\mathbf{x})}{\gamma^4(1-\mathbf{n}\cdot\mathbf{v}(t,\mathbf{x}))^4} + \frac{1}{6}\frac{\rho\lambda(t,\mathbf{x})g^{\mu\nu}\delta(e,p)}{\gamma^2(1-\mathbf{n}\cdot\mathbf{v}(t,\mathbf{x}))^2} \right) dS(\mathbf{n})\,. \end{aligned} \tag{A-2}$$

Similarly one can easily see that

$$\rho(t,\mathbf{x}) = \frac{2}{\lambda}\int_{\mathbb{R}^3} f(t,\mathbf{x},\mathbf{q})\frac{d^3q}{|\mathbf{q}|} = \frac{1}{4\pi} \oint\limits_{\partial B(0,1)} \frac{\rho(t,\mathbf{x})}{\gamma^2(1-\mathbf{n}\cdot\mathbf{v}(t,\mathbf{x}))^2} dS(\mathbf{n})\,. \tag{A-3}$$

Here $\mathbf{n} = \frac{\mathbf{q}}{|\mathbf{q}|}$ is the unit vector in direction of $\mathbf{q}$ and $B(\mathbf{x}_0, r)$ is the ball with radius r and center $\mathbf{x}_0$ with boundary $\partial B(\mathbf{x}_0, r)$. Note that n^μ is not a four-vector and $n^0 = 1$.

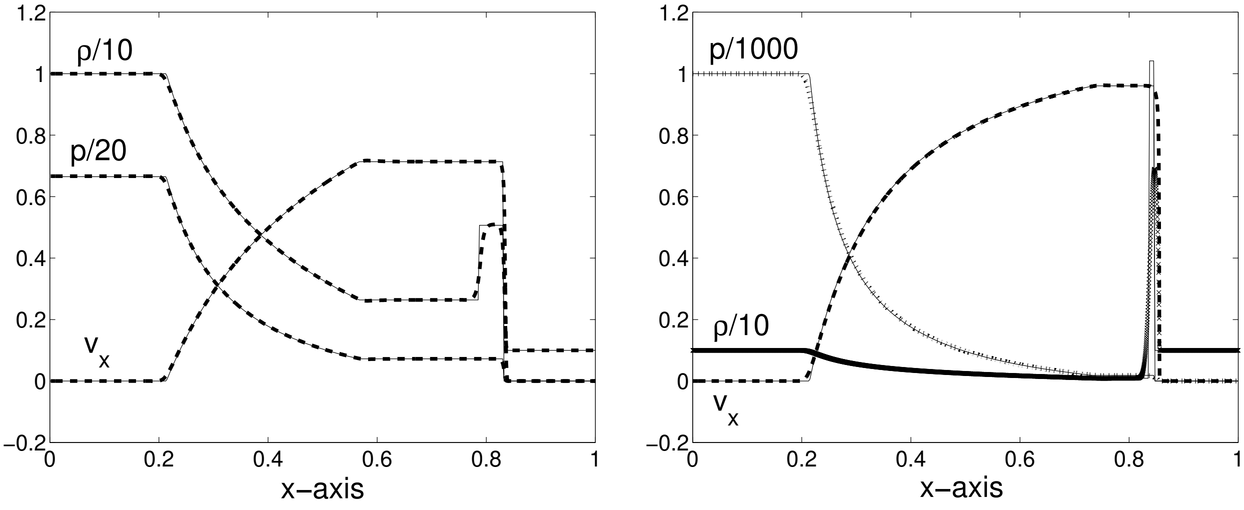

(a) (b)

Figure 2: Results of problem 1 & 2 at times $t = 0.4$ and $t = 0.35$, respectively.

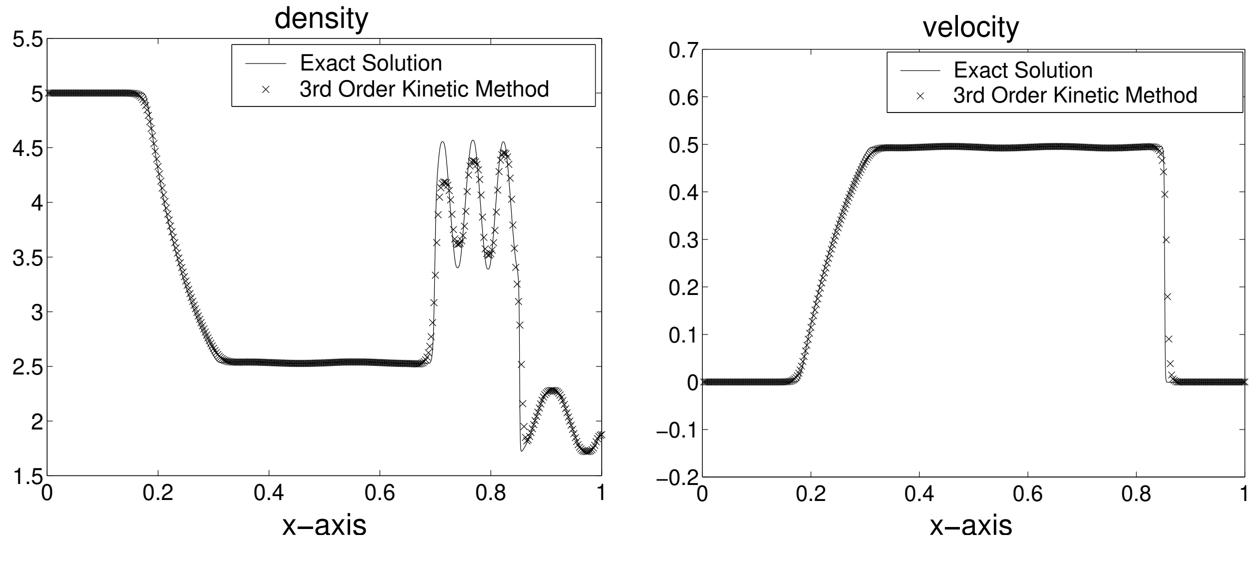

Figure 3: Results of problem 3 at time $t = 0.35$.

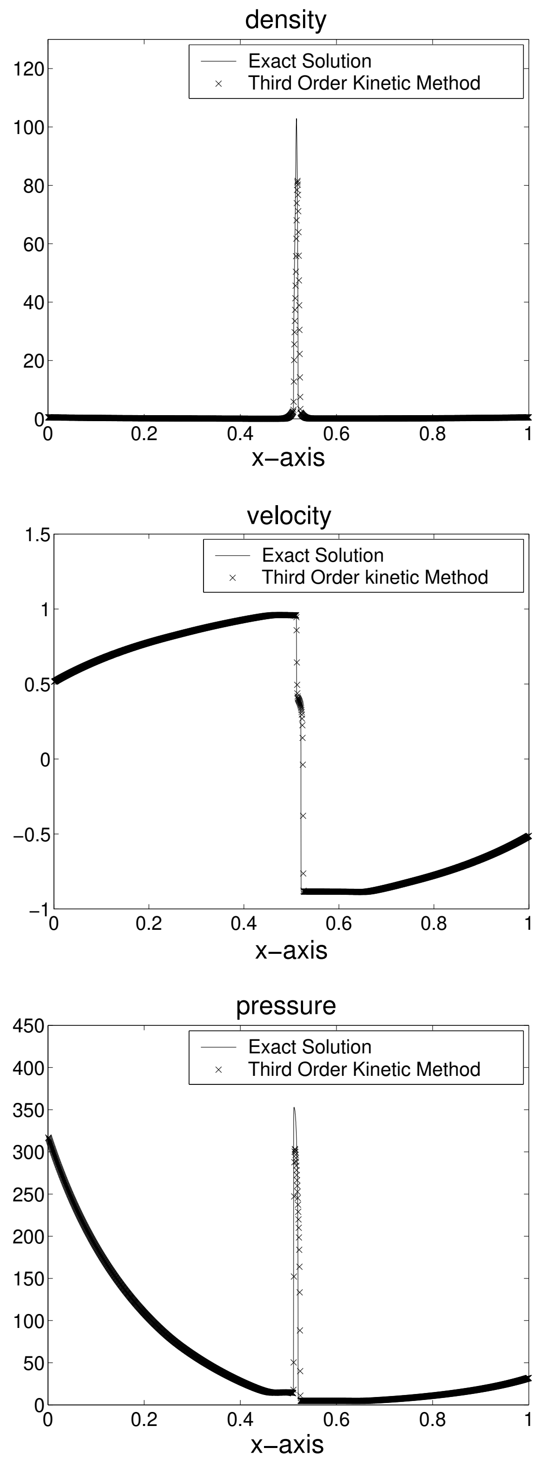

Figure 4: Results of problem 4 at time $t = 0.43$.

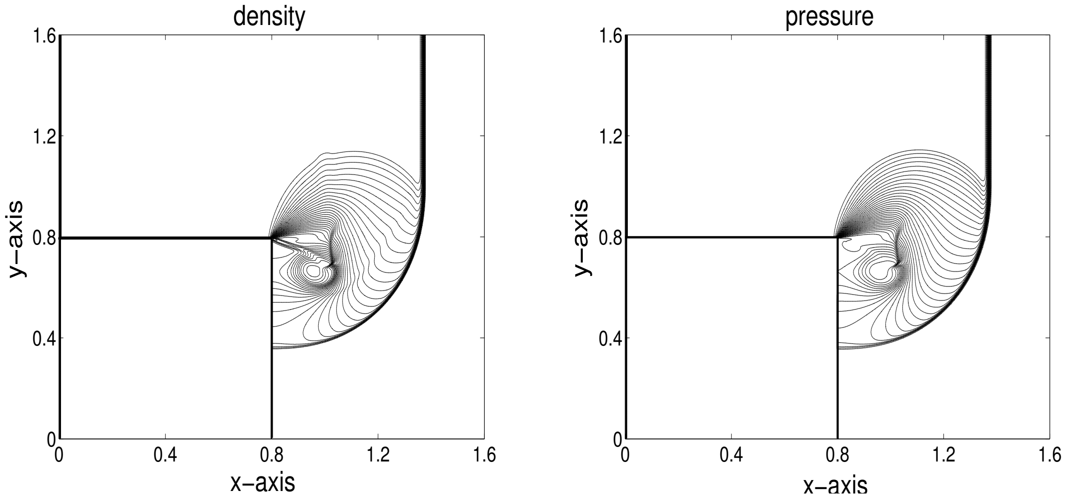

Figure 5: Results of problem 5 at time $t = 1.7$.

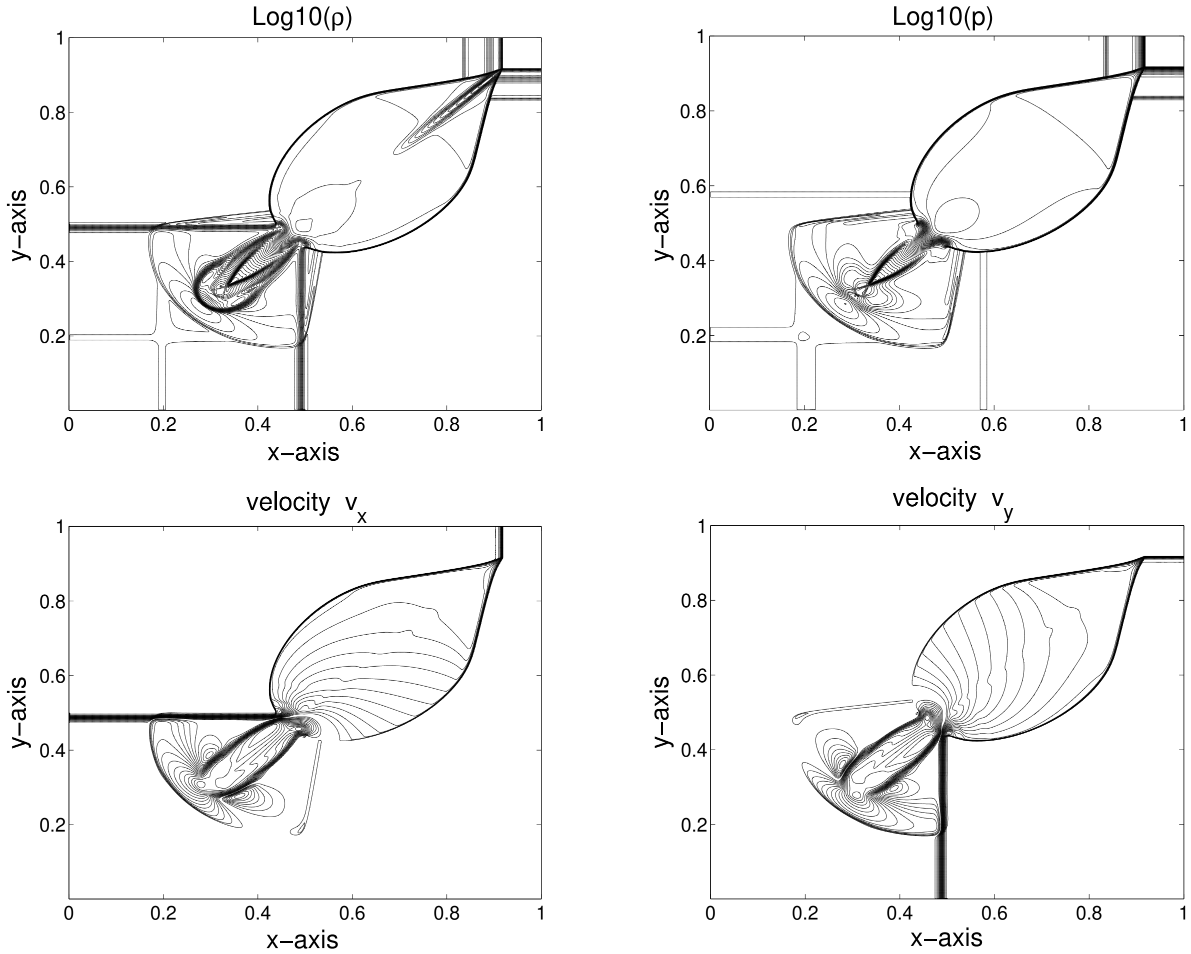

Figure 6: Results of problem 6 at time $t = 0.4$.

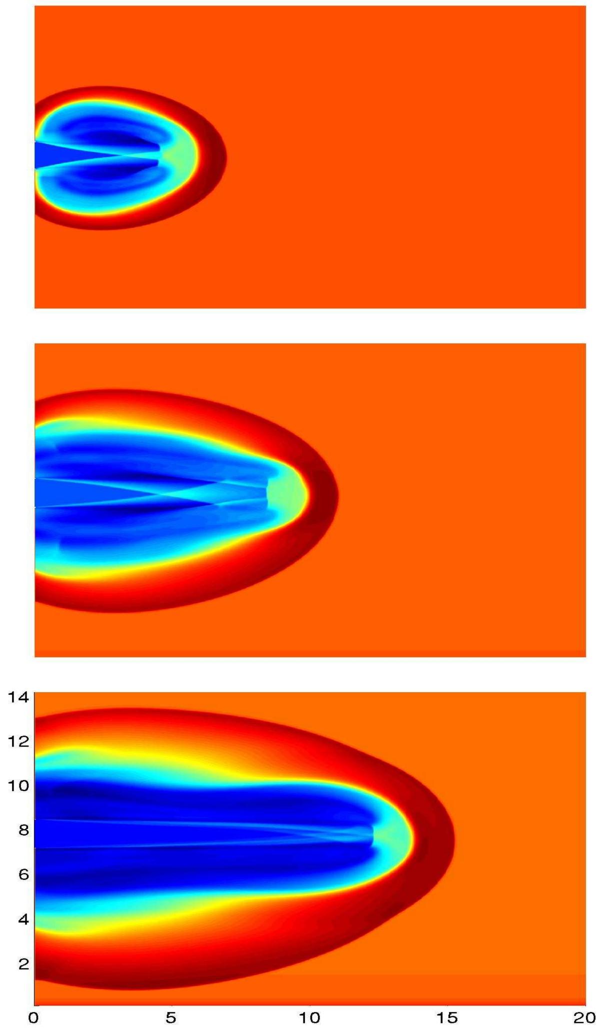

Figure 7: Relativistic jet in problem 7 at times $t = 15, 25, 35$, respectively.

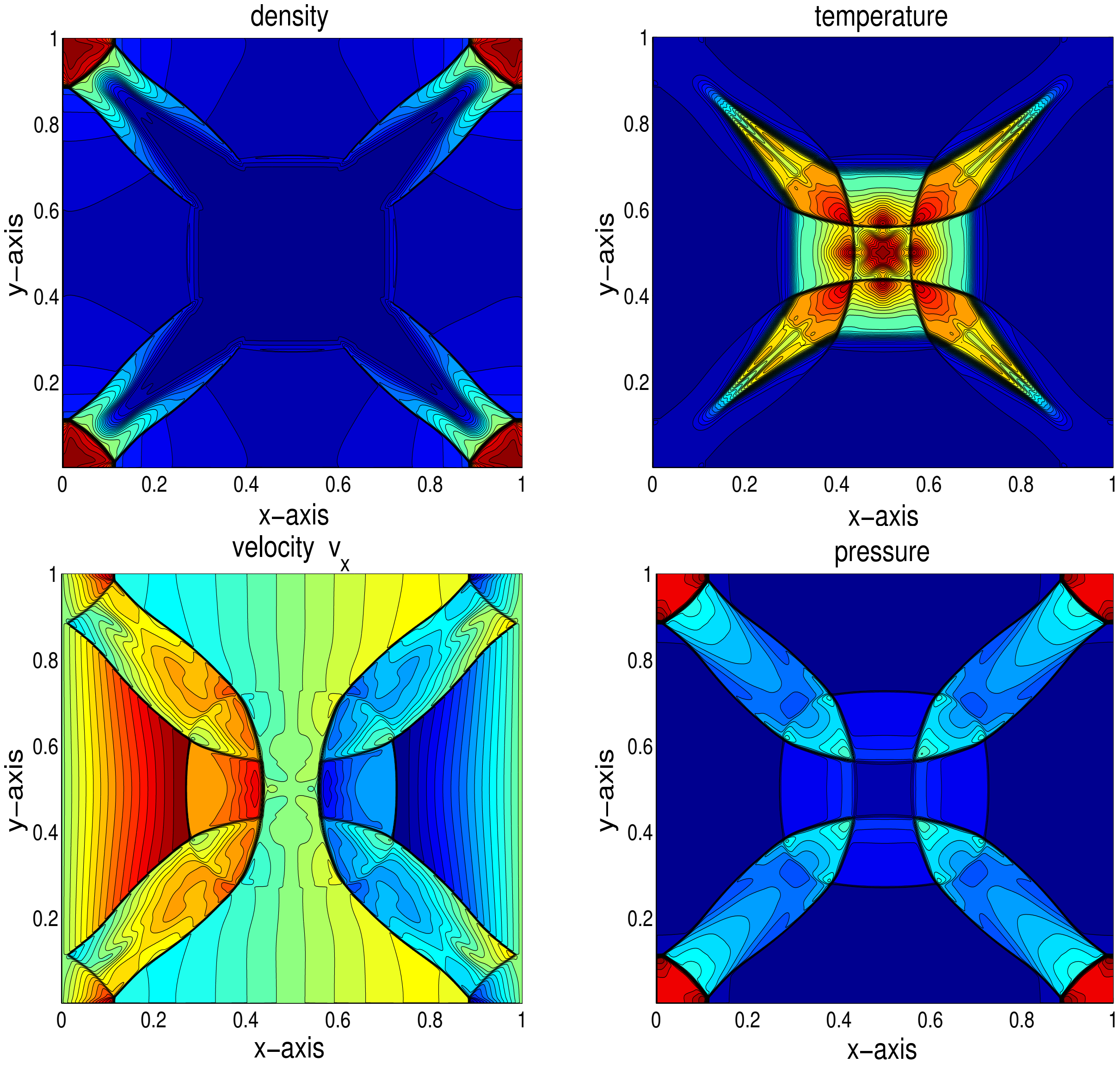

Figure 8: Results of problem 8 at time $t = 1.0$.

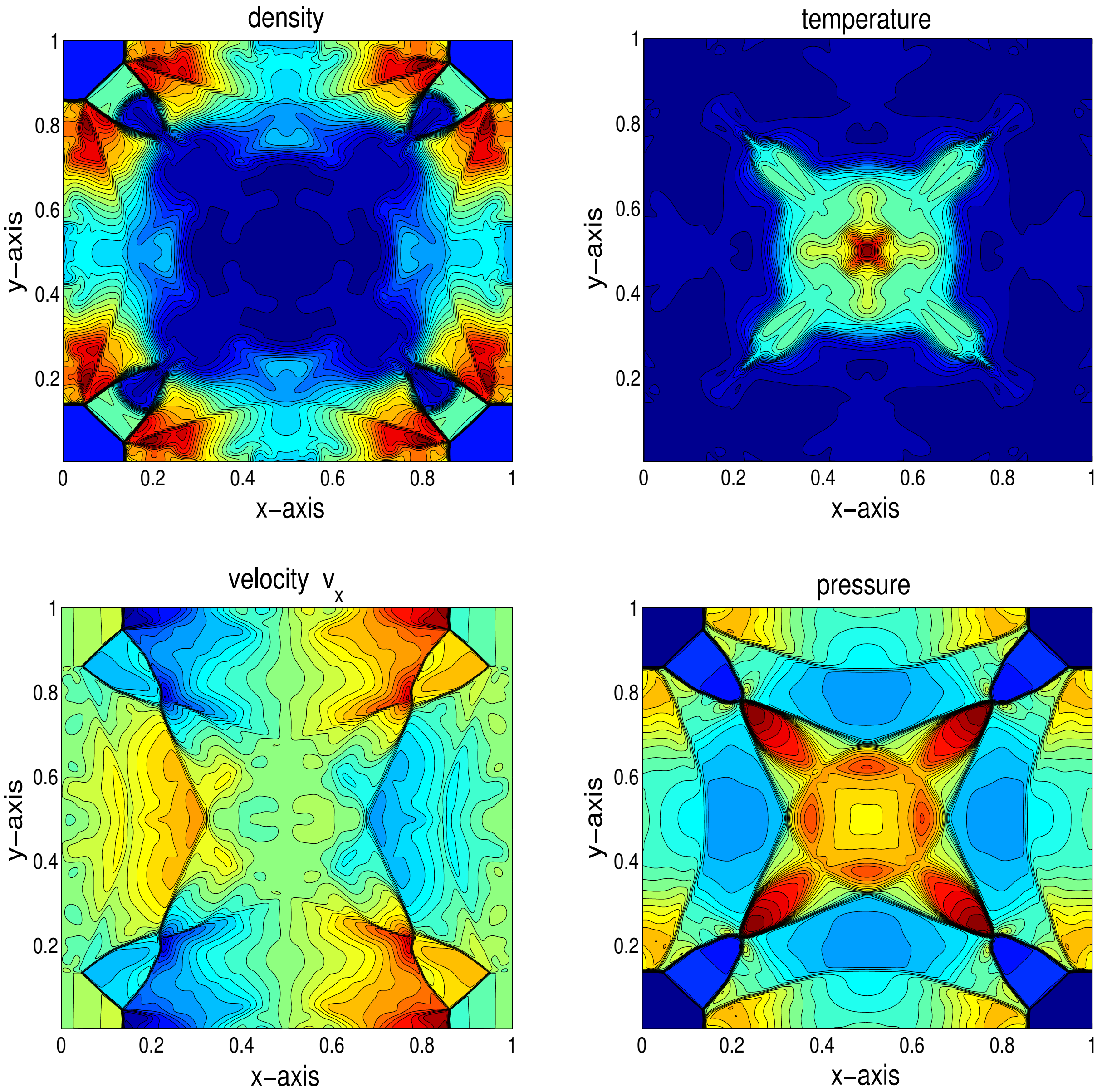

Figure 9: Results of problem 8 at time $t = 2.0$.

References

[1] M.A. Aloy, J.M$^{\underline{a}}$ Ibáñez, J.M$^{\underline{a}}$ Martí, E. Müller, "GENESIS: A high-resolution code for 3d relativistic hydrodynamics", *Astrophys. J.* **122** (1999) pp. 151-166.

[2] M. C. Begelman, R. D. Blandford, and M. J. Rees, " Theory of extragalactic radio sources", *Rev. Mod.Phys.* **56**, (1984), pp. 255-351.

[3] L.P. Csernai, " Introduction to relativistic heavy ion collisions", Wiley, Chichester, New York (1994).

[4] S. M. Deshpande and P.S. Kulkarni, "New developments in kinetic schemes", *Computer math. Applic.*, **35**, (1998) pp. 75-93.

[5] S. M. Deshpande, "Kinetic flux splitting schemes", *In Computational Fluid Dynamics Review 1995, (Edited by M. Hafez and K. Oshima)*, John Wiley & Sons, (1995).

[6] R. Donat, A. Marquina, "Capturing shock reflections: An improved flux formula", *J. Comp. Phys.,* **125** (1996) pp. 42-58.

[7] F. Eulderink, and G. Mellema, "General relativistic hydrodynamics with a Roe solver", *Astron. Astrophys. Suppl.,* **110** (1995) pp. 587-623.

[8] E. Godlewski and P.A. Raviart, "Numerical approximation of hyperbolic systems of conservation laws", *Springer*, (1996).

[9] A. Harten, P.D. Lax and B. van Leer, "On upstream differencing and Godunov-type schemes for hyperbolic conservation laws", *SIAM Review*, **25**, (1983) pp. 35-61.

[10] G.S. Jiang and C.W. Shu, "Efficient implementation of weighted ENO schemes", *J. Comput. Phys.* **126**, (1996), pp. 202-228.

[11] A. Jameson, W. Schmidt, and E. Turkel, "Numerical solutions of the Euler equations by finite volume methods using Runge-Kutta time-stepping scheme", AIAA81-1259, (1981).

[12] F. Jüttner, "Das Maxwellsche Gesetz der Geschwindigkeitsverteilung in der Relativtheorie", *Ann. Phys.* (Leipzig), **34**, (1911) pp. 856-882.

[13] J.M$^{\underline{a}}$ Martí, E. Müller, "Numerical hydrodynamics in speical relativity", *Living Reviews in Relativity* **2** (1999) p. 1-101.

[14] M. Kunik, S. Qamar and G. Warnecke, "Kinetic schemes for the ultra-relativistic Euler equations", *J. Comput. Phys.* **187**, (2003), pp. 572-596.

[15] M. Kunik, S. Qamar and G. Warnecke, "Kinetic schemes for the relativistic gas dynamics", *Num. Math.* **97**, (2004), pp. 159-191.

[16] M. Kunik, S. Qamar and G. Warnecke, "A BGK-type kinetic flux-vector splitting schemes for the ultra-relativistic relativistic gas dynamics", Preprint Nr. **4**, Otto-von-Guericke University Magdeburg, Germany, (2003), accepted in *J. Sci. Comput.*, (2003).

[17] L. D. Landau & E. M. Lifshitz "Fluid Mechanics", Pergamon Press, New York, (1987).

[18] A. Kurganov and P. D. Levy, "A third-order semidiscrete central scheme for conservation laws and convection-diffusion equations", *SIAM. J. Sci. Comput.* **22**, (2000), pp. 1461-1488.

[19] P. D. Levy, G. Puppo, and G. Russo, "Compact central WENO schemes for multidimensional conservation laws ", *SIAM. J. Sci. Comput.* **22**, (2000), pp. 656-672.

[20] J.C. Mandal and S.M. Deshpande, "Kinetic flux -vector splitting for Euler equations", *Computer & Fluids,* **23**(**2**), (1994) pp. 447-478.

[21] J.Mª Martí, E. Müller, J.A. Font, J.Mª Ibáñez, "Morphology and dynamics of highly supersonic relativistic jets", *Astrophysics. J.* **448** (1995) L105-L108.

[22] J.Mª Martí, E. Müller, "Extension of the piecewise parabolic method to one-dimensional relativistic hydrodynamics", *J. Comp. Phys.,* **123** (1996) pp. 1-14.

[23] J.Mª Martí, E. Müller, "Numerical hydrodynamics in speical relativity", *Living Reviews in Relativity* **2** (1999) p. 1-101.

[24] I. F. Mirabel and L. F. Rodriguez, "A superluminal source in the galaxy", *Nature* **371**, (1994), pp. 46.

[25] P. Mészáros and M. J. Rees, "Tidal heating and mass loss in neutron star binaries - Implications for gamma-ray burst models", *APJ.* **397**, (1992), pp. 570-575.

[26] S. Osher and F. Solomon, "Upwind difference schemes for hyperbolic systems of conservation laws", *Math. Comput.,* **38** (1982), pp. 339-374.

[27] T. Piran, A. Shemi and R. Narayan, "Hydrodynamics of relativistic fireballs", *Mon. Not. R. Astron. Soc.,* **263** (1993), pp. 861-867.

[28] P.L. Roe, "Approximate Riemann Solvers, parameter vectors and difference scheme", *J. Comput. Phys.* **43,** 357 (1981).

[29] V. Schneider, U. Katscher, D. H. Rischke, B. Waldhauser, J.A. Maruhn, C.-D. Munz, "New algorithms for ultra-relativistic numerical hydrodynamics", *J. Comp. Phys.,* **105**, (1993) pp. 92-107.

[30] T. Tang and K. Xu, "A high-order gas-kinetic method for multidimensional ideal magnetohydrodynamics", *J. Comput. Phys.* **165**, (2000), pp. 69-88.

[31] E.F. Toro, "Riemann solvers and numerical method for fluid dynamics", Second Edition, Springer-Verlag, (1999).

[32] M. van Dyke, "An album of fluid motion", The Parabolic press, Stanford, California, (1982).

[33] B. van Leer, "Towards the ultimate conservative difference scheme V. A second order sequel to Godunov's method", *J. Comput. Phys.* **32**, (1979), pp. 101-136.

[34] P.R. Woodward, and P. Colella, "The numerical simulation of two-dimensional fluid flow with strong shocks", *J. Comp. Phys.* **54**, (1984) pp. 115-173.

[35] K. Xu, "Gas kinetic schemes for unsteady compressible low simulations", 29th CFD, Lecture Series (1998).

[36] K. Xu, "Gas-kinetic theory based flux slitting method for ideal magnetohydrodynamics", *J. Comput. Phys.* **153**, (1999), pp. 334-352.

[37] K. Xu, L. Martinelli and A. Jameson, "Gas-kinetic finite volume methods, flux-vector splitting and artificial diffusion ", *J. Compute. Phys.*, **120** (1995), pp. 48-65.

[38] J. Y. Yang, M. H. Chen, I. N. Tsai, and J. W. Chang, "A kinetic beam scheme for relativistic gas dynamics", *J. Comput. Phys.* **136** (1997), pp. 19-40.

[39] L. Del Zanna and N. Bucciantini, "An efficient shock-capturing central-type scheme for multidimensional relativistic flows, I. Hydrodynamics", *A&A* **390**, (2002), pp. 1177-1186.